materials proceedings

MDPI

Proceeding Paper

The Influence of Casting Static Compaction Pressure on Carbonated Reactive Magnesia Cement (CRMC)-Based Mortars †

Erick Grünhäuser Soares [1,*], João Castro-Gomes [1] and Manuel Magrinho [2]

[1] Centre of Materials and Building Technologies (C–MADE), Department of Civil Engineering and Architecture, University of Beira Interior (UBI), 6201-001 Covilhã, Portugal
[2] Centre of Materials and Building Technologies (C–MADE), Department of Chemistry, University of Beira Interior (UBI), 6201-001 Covilhã, Portugal
* Correspondence: e.grunhauser@ubi.pt
† Presented at the 10th MATBUD'2023 Scientific-Technical Conference "Building Materials Engineering and Innovative Sustainable Materials", Cracow, Poland, 19–21 April 2023.

Abstract: The current study evaluates the influence of the static compaction pressure applied during the casting process on Carbonated Reactive Magnesia Cement-based mortars. For this purpose, mortars, embodying biomass fly ash as filler, were designed and moulded through static compaction pressures of 10, 30, 50, and 70 MPa. The moulded specimens were submitted to an accelerated carbonation curing period of 24 h under controlled conditions. The devised mortars were evaluated through compressive strength tests, and their microstructure was assessed through Mercury Intrusion Porosimetry (MIP), Thermogravimetry and Derivative Thermogravimetry (TG-DTG), and Fourier-transform Infrared Spectroscopy (FTIR) analyses. The results showed that the increment in the static compaction pressure during the specimens' casting process not only led the mortars to reduce their porosity by up to ~30% and increase their compressive strength by up to ~58% (from 19.8 MPa to 31.2 MPa) but also that such a change seems to hinder the CO_2 diffusion into the specimens' core, thus resulting in a lower content of carbonated products. In addition, the MIP analyses demonstrated that the static compaction pressure applied in the mortar casting process changes the pores' characteristics, while TG-DTG and FTIR analyses provided evidence that the devised mortars were carbonated to a certain degree. Therefore, this work demonstrated that Carbonated Reactive Magnesia Cement-based mortars are highly influenced by the static compaction pressure applied during the casting process, at least up to a certain value.

Keywords: Carbonated reactive magnesia cement; CO_2 mineralisation; influencing factor; static compaction pressure; biomass fly ash

Citation: Grünhäuser Soares, E.; Castro-Gomes, J.; Magrinho, M. The Influence of Casting Static Compaction Pressure on Carbonated Reactive Magnesia Cement (CRMC)-Based Mortars. *Mater. Proc.* **2023**, *13*, 5. https://doi.org/10.3390/materproc2023013005

Academic Editors: Katarzyna Mróz, Tomasz Tracz, Tomasz Zdeb and Izabela Hager

Published: 13 February 2023

1. Introduction

Carbonatable binders have emerged as one of the alternative binders to Portland Cement-based materials that could assist in the global trend of reducing CO_2 emissions [1]. Carbonated Reactive Magnesia Cement (CRMC), which is based on the transition of Magnesia to Hydrated Magnesium Carbonates (HMCs), such as Dypingite ($Mg_5(CO_3)_4(OH)_2 \cdot 5H_2O$), Hydromagnesite ($Mg_5(CO_3)_4(OH)_2 \cdot 4H_2O$), and Nesquehonite ($MgCO_3 \cdot 3H_2O$), through Accelerated Carbonation Curing (ACC) [2–5], is among this group of binders.

However, the success of the ACC of CRMC-based materials is highly dependent on a wide range of factors, such as the conditions to which the fresh CRMC-based material is exposed (e.g., CO_2 environment, curing temperature, period of exposition, and relative humidity), the raw materials' properties (e.g., Magnesia source, Magnesia calcination history, and type of aggregates used), the blend design (e.g., water content, pH, additives used, and the use of Magnesia replacement), and both geometry and porosity of the fresh material [6]. In addition to the previously mentioned carbonation-curing influencing

factors, the compaction pressure on the specimens' casting process of carbonatable binders is another factor that may significantly influence the compressive strength obtained in this group of binders, mainly due to its influence on the porosity of the material [7]. However, it seems that this approach has not yet been investigated regarding CaO-based materials.

For this purpose, an exploratory approach was developed aiming to investigate how a CRMC-based mortar exposed to ACC behaves when modifications in the static compaction pressure of the casting process are made. A total of 16 specimens were produced and tested for four different static compaction pressures (i.e., 10, 30, 50, and 70 MPa). Moreover, the mixture, the production method, and the ACC conditions were defined based on previous studies [8–10], which used a reactive compound (MgO), a waste-based material as filler, and sand as fine aggregate to produce CRMC-based mortars that were moulded through static compaction and cured under pressurized ACC for 24 h under controlled conditions.

With the aim of understanding the CRMC-based mortar development, the devised mortars were then evaluated through compressive strength tests, Mercury Intrusion Porosimetry (MIP) analysis, Thermogravimetry and Derivative Thermogravimetry (TG-DTG), and Fourier-transform Infrared Spectroscopy (FTIR) analyses.

2. Materials and Methods

2.1. Materials

Reactive Magnesia (r-MgO), with the commercial name "Calcined Magnesite 92/200", was supplied by Richard Baker Harrison Ltd., Liverpool, England. Its reactivity was recorded as 48 s [11], thus classifying it as medium-reactive magnesia [12]. Biomass fly ash (BFA) was used as it was received and consisted of residual energy production material from a burning forestry source, which was supplied by Central de Biomassa do Fundão, Unipessoal LDA, Fundão, Portugal. The fine aggregate used was river sand (RS), supplied by Tabal-Sepor Areias e Argamassas LDA, Salvaterra de Magos, Portugal, which presented a medium particle diameter (D_{50}) of 1.08 mm and a coefficient of uniformity of 3.02. It is important to note that RS was employed in the devised materials to represent their true condition aside from facilitating the CO_2 diffusion into the specimens' core although the use of fine aggregates is known to cause quartz contamination that, in turn, may lead to awkwardness in phase identification.

The raw materials' oxide composition is displayed in Table 1, which was estimated through Energy-dispersive X-ray spectroscopy (EDX) analysis (S-3400N Spectrometer, Hitachi, Tokyo, Japan). The raw materials' physical properties, namely true density, Blaine fineness, and Loss on Ignition (LOI), are shown in Table 2. The true density was determined through a helium gas displacement pycnometer equipment (AccuPyc 1330, Micromeritics, Norcross, GA, USA). The Blaine fineness of the powders (r-MgO and BFA) was determined using a Blaine air permeability apparatus (BSA1, Acmel Labo, Champlan, France). The LOI was obtained through TG-DTG analysis (SDT Q-50, TA Instruments, New Castle, DE, USA).

Table 1. Oxide composition.

Raw Material	Oxide Composition											
	Na_2O	MgO	Al_2O_3	SiO_2	P_2O_5	SO_3	Cl^-	K_2O	CaO	TiO_2	MnO	Fe_2O_3
r-MgO	-	93.3	-	1.6	-	-	-	-	3.5	-	-	1.6
BFA	1.6	5.7	20.3	35.1	2.4	2.7	0.5	8.9	14.9	0.7	0.7	6.3
RS	3.3	0.7	13.2	76.5	-	-	-	3.4	1.4	-	-	1.6

Table 2. Physical properties.

Raw Material	Physical Properties		
	True Density (g/cm^3)	Blaine Fineness (cm^2/g)	LOI (%) at 1000 °C
r-MgO	3.0	6263	10.4
BFA	2.3	4029	7.5
RS	2.6	-	3.7

2.2. Mixture Design and Production of Specimens

The mixture labels are presented in Table 3, and they consist of a binder-to-sand volume ratio of 1:3, a water-to-solids-in-the-binder mass ratio of 0.41, where the solids in the binder are composed of r-MgO and BFA in a volume ratio of 2:3. Four cubic-shaped specimens with 40 mm edge were produced for each mixture label based on the methodology described in recent studies [8–10]. A pressurised ACC chamber of approximately 75 litres was used, and an initial partial vacuum pressure of 0.2 bar was applied. Afterwards, the following ACC conditions were provided: CO_2 concentration > 99%; CO_2 partial pressure = 0.7 bar; T = 60 ± 2 °C; relative humidity (RH) > 99%; and AAC period = 24 h. Following the AAC period, the CRMC-based specimens were immediately stored in lab room conditions (20 ± 2 °C and an RH of 60 ± 5%) for 24 h to cool them before compressive strength testing.

Table 3. Mixture labels.

Mixture Label	Raw Material (vol. %)			w/b	Static Compaction Pressure (MPa)
	r-MgO	BFA	RS		
M.P-10	10.0	15.0	75.0	0.41	10
M.P-30					30
M.P-50					50
M.P-70					70

2.3. Assessment of the CRMC-Based Mortars Developed

Compressive strength tests were carried out through uniaxial loading in triplicate, and their average was reported. A compression machine with digital readout and self-centering platens, operated at a constant loading rate of 1.35 kN/s, was used (ADR Touch 3000 BS EN, ELE International, Leighton Buzzard, UK). The tested material was collected for further microstructural investigations (TG-DTG and FTIR analyses). MIP analyses were performed using a mercury porosimeter (AutoPore IV 9500, Micromeritics, Norcross, GA, USA), with maximum and minimum applied pressures of ~34,000 psia and ~0.5 psia, respectively, thus corresponding to a minimum pore size of 5 nm and a maximum pore size of 345 μm. A mercury surface tension of 480 mM/m was applied. Mercury-solid contact angles for intrusion and extrusion were defined as 130° and 104°, respectively. Specimen fragments with a mass range of 1.50–1.90 g were obtained by sawing the specimens that were not subjected to the compressive strength test to acquire more accurate data for MIP analysis [13]. Before being tested, these fragments were stored in a glass desiccator containing silica gel for seven days to ensure the removal of moisture and ensure the effectiveness of the test. TG-DTG analyses were performed from ambient temperature (20 ± 2 °C) to 1000 °C at a heating rate of 20 °C/min under nitrogen flow (SDT Q-50, TA Instruments, New Castle, DE, USA). The material tested consisted of ~7 mg of particles passing through a 63 μm sieve, which were first submitted to a drying stage of 24 h at 60 °C to avoid the overlapping effect of free water release with the dehydration step in the TG-DTG curves. FTIR data were obtained by recording the infrared spectrum from 600 to 1600 cm^1 using a FTIR Spectrometer apparatus (Nicolet iS10 with a Smart ATR accessory, Thermo Fisher Scientific, Waltham, MA, USA).

3. Results and Discussion

The average compressive strength results of each mixture label are shown in Figure 1 and Table 4. The specimens reached a compressive strength of 19.8 MPa to 31.2 MPa. It was noticed that a change in only one parameter of the casting process can enhance the compressive strength results by ~58% when comparing M.P-10 with M.P-70. However, it was also observed that the degree of enhancement in compressive strength reduces as the static compaction pressure of the casting process increases. Thus, when comparing the M.P-50 with M.P-70, the compressive strength gain was only 1.5%. Therefore, it must be highlighted that the static compaction pressure applied in the casting process plays an important role in the strength development of CRMC-based materials but this strength gain

may be almost negligible for static compaction pressures above 50 MPa. Similar behaviour was observed in steel slag-based CO_2-cured pastes [7]. Furthermore, the calculated standard deviation of the compressive strength results indicates that the materials devised for this study exhibit a high degree of homogeneity.

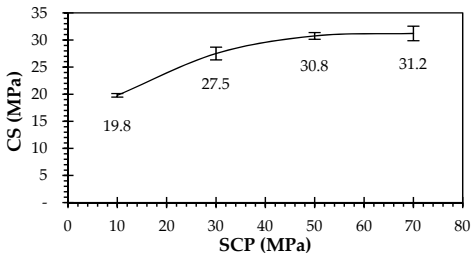

Figure 1. Static compaction pressure (SCP) vs. compressive strength (CS).

Table 4. Compressive strength results.

Parameter		Mixture Label			
		M.P-10	M.P-30	M.P-50	M.P-70
Compressive strength (MPa)		19.79	27.50	30.75	31.21
Standard deviation (MPa)		0.32	1.19	0.62	1.34
Compressive strength enhancement/weakening (%) comparing with	M.P-10	–	38.96	55.38	57.71
	M.P-30	−28.04	–	11.82	13.49
	M.P-50	−35.64	−10.57	–	1.50
	M.P-70	−36.59	−11.89	−1.47	–

The porosity and other parameters obtained throughout the MIP analysis are summarized in Table 5 and shown in Figure 2.

Table 5. MIP results.

Parameter		Mixture Label			
		M.P-10	M.P-30	M.P-50	M.P-70
Porosity (%)		22.34	18.99	16.90	15.80
Average pore diameter (μm)		0.07	0.05	0.06	0.05
Critical diameter (μm)		25.60	12.36	5.38	11.76
Bulk density at 14.50 psia (g/mL)		2.11	2.08	2.11	2.13
Apparent (skeletal) density (g/mL)		2.45	2.48	2.48	2.47
Pores typology (%) [14]	Mesopores (0.002−0.05 μm)	19.44	23.64	22.11	22.03
	Macropores (0.05−10 μm)	33.56	53.06	60.80	57.41
	Air voids/cracks (≥10 μm)	47.00	23.30	17.09	20.56

The analyses revealed that the mixture labels hold different porosity indices ranging from 15.80% to 22.34%. These results show that for the range of compaction pressure applied in the mortars' casting process of this study, higher values of static compaction pressure led to lower porosity indices and higher compressive strength results, as shown in Figure 2a. The M.P-30, M.P-50, and M.P-70 mixtures presented similar indices of mesopores, macropores, and air voids/cracks, while M.P-10 exhibited a much higher index of air voids/cracks, a lower index of macropores, and a similar index of mesopores than the rest (Figure 2c). Thus, such behaviour indicates that the compaction pressure applied in the mortars' casting process affects the pore typology up to a certain degree and acts especially on the transition of air voids/cracks to macropores and scarcely affects the increment of the mesopores index. Regarding the critical diameter (∅c), the results show that M.P-10 presented a much higher value than the other mixtures (M.P-10 = 25.6 μm; M.P-30 = 12.4 μm; M.P-50 = 5.4 μm; M.P-70 = 11.8 μm), where such behaviour seems to be related to the lower static compaction pressure applied in the casting process. Interestingly,

M.P-50 exhibited a critical diameter about two times lower than the one observed in M.P-70. Such behaviour may be attributed to the BFA pores since a peak in this diameter size is also present in other mixtures. The biomass fly ash was used as it was received, so differences in the pore structure of the raw materials may be found. Therefore, MIP results demonstrated that the static compaction pressure applied during the casting process plays an important role in the mortar's porosity index and in the characteristics of its pores which, in turn, affect the compressive strength results.

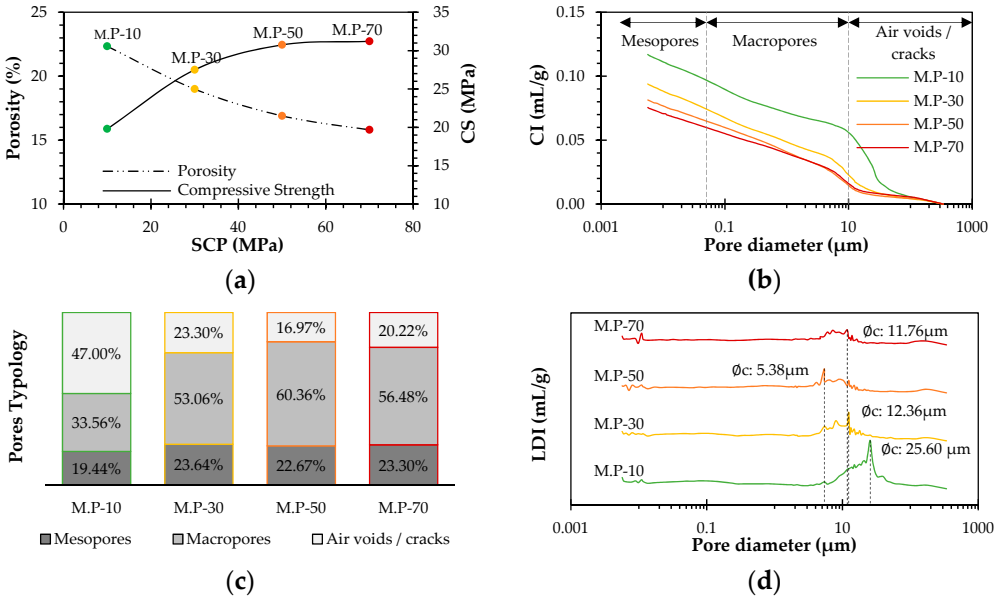

Figure 2. (**a**) Static compaction pressure (SCP) vs. compressive strength (CS) and porosity; (**b**) Cumulative intrusion (CI) vs. pore diameter; (**c**) Pores typology (%); (**d**) Log differential intrusion (LDI) vs. pore diameter.

The TG-DTG analyses (Figure 3) show that the mass loss of the devised materials was gradual, reaching the highest mass loss rate at a temperature range between 300 and 550 °C (Table 6). In this temperature range, the M.P-10 mixture had the highest index of mass loss (~15%), while the M.P-30, M.P-50, and M.P-70 lost ~12, 10, and 9% of their initial masses, respectively. Interestingly, the mass loss for this temperature interval does not follow the typical behaviour of compressive strength development in CRMC-based materials, since the mixture labels with lower compressive strength results had higher mass losses in the region of ~300–550 °C, thus indicating that more HMCs and carbonates were formed in these mixtures, probably due to the higher porosity index in the fresh moulded specimen thanks to the lower static pressure applied in their casting process. The DTG curves (Figure 3a) exhibit two initial peaks, which are attributed to the free water evaporation and dehydration of water bound to the HMCs [15–17]. The region between 300 and 550 °C presents a higher peak at ~420 °C, which refers to the overlapping curves of the dehydroxylation of Brucite [15,18,19] and Dypingite [15,18], as well as the decarbonisation of Hydromagnesite [20] and Nesquehonite [15,18,21], whereas the smaller peak at ~460 °C and the mass loss in the range of 450 to 600 °C correspond to the decarbonisation of Magnesite [19,22] and/or of undefined HMCs [4]. In turn, the last peak may be caused by the decarbonisation of Calcite and/or amorphous carbonates [23–25]. Finally, the TG-DTG analyses indicate that the four designed mortars were carbonated to a certain degree, in which the magnesia hydration and carbonation seem to be favourably affected by using a lower static compaction pressure in the casting process since the mass loss in the temperature range of 300−550 °C is higher as the applied static compaction pressure is lowered. Such a trend may occur due to a lower porosity index which negatively influences

the CO_2 diffusion into the core of the designed materials, thus hindering the formation of HMCs.

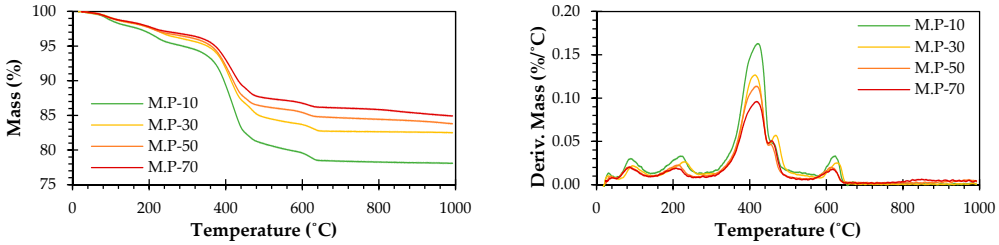

Figure 3. (**a**) TG curves; (**b**) DTG curves.

Table 6. Mass loss (%) in TG-DTG.

Mixture Label	Mass Loss (%) in TG-DTG by Temperature Range			
	25−300 °C	300−550 °C	550−1000 °C	∑
M.P-10	5.19	14.63	2.09	21.92
M.P-30	4.07	11.77	1.63	17.47
M.P-50	3.66	10.41	2.10	16.17
M.P-70	3.34	9.43	2.28	15.05

The recorded FTIR spectra data of the four mixtures are exhibited in Figure 4. Despite the low intensity of the observed bands that may be attributed to the low MgO content (10 vol. %), some considerations may be made as follows: the absorbance bands located at ~680, 855, 880, 1420, and 1485 cm^{-1} indicate the presence of HMCs such as Nesquehonite, Hydromagnesite, and Dypingite [26–29], while the bands at ~720 and 1460 cm^{-1} could be attributed to the presence of Lansfordite [28]. Therefore, these absorbance bands may indicate that part of the r-MgO in the mixture was carbonated to a certain degree. Furthermore, the unidentified absorbance bands located between 800 and 1200 cm^{-1} may be due to the presence of MSH gels [30], which, along with the HMCs, tend to fill the cementitious matrix voids contributing to the enhancement in compressive strength [26].

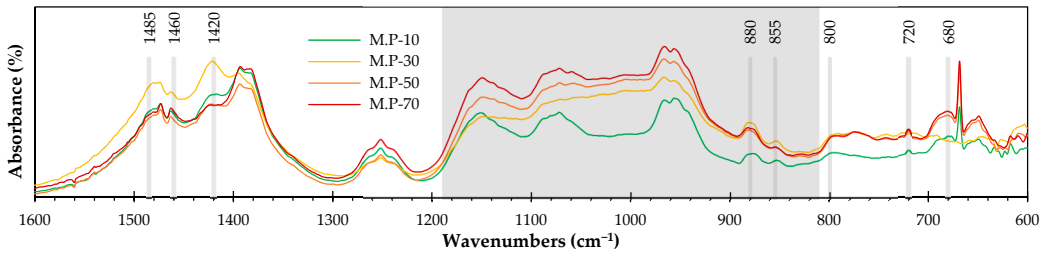

Figure 4. FTIR curves.

4. Conclusions

This work presented how CRMC-based mortars behave when changes in static compaction pressure on their casting process are made. For this purpose, the compressive strength of the developed mortars was evaluated, and MIP, TG-DTG, and FTIR analyses were carried out. Therefore, the main contributions of this study are as follows: higher values of static compaction pressure used during the casting process resulted in higher compressive strengths for the mortars developed and lower formation of HMCs. However, as the static compression pressure increases, the strength gain decreases, thus making it almost ineffective when applied at pressures greater than 50 MPa (i.e., M.P-70). MIP results showed that the static compaction pressure applied during the casting process of

the devised mortars plays an important role in the porosity index and characteristics of the pores, thus affecting the results of the compressive strength obtained. TG-DTG and FTIR analyses indicated that the devised mortars were carbonated to a certain degree. More studies related to the microstructure, such as X-ray diffraction (XRD), and Scanning Electron Microscopy (SEM) with Energy Dispersive X-Ray Analysis (EDX) on the devised mortars analyses, should be carried out to better understand these materials.

Finally, the casting and the accelerated carbonation curing processes established and used in this study limit the suitability of the created mortars to the production of pre-cast building materials only.

Author Contributions: E.G.S.: Conceptualization, Methodology, Investigation, Writing—original draft, Writing—review & editing. J.C.-G.: Writing—review & editing, Supervision, Project administration, Funding acquisition. M.M.: Writing—review & editing. All authors have read and agreed to the published version of the manuscript.

Funding: Portuguese national funds partially financed this work through FCT, Foundation for Science and Technology, IP, within the research unit C-MADE, Centre of Materials and Building Technologies (CIVE-Central Covilhã-4082), University of Beira Interior, Portugal. This research was also partially funded by FCT grant number 2022.09813.BD.

Institutional Review Board Statement: Not applicable.

Informed Consent Statement: Not applicable.

Data Availability Statement: Not applicable.

Acknowledgments: The authors acknowledge Engineer Ana Paula Gomes from the Optical Centre of UBI (COUBI) for her contribution in carrying out the EDX analyses, and Engineer Carlos Alegria and Engineer Paulo Godinho from Magestop, Central de Biomassa do Fundão, for providing the biomass ashes used in this research. The publication cost of this paper was covered with funds from the Polish National Agency for Academic Exchange (NAWA): "MATBUD'2023 - Developing international scientific cooperation in the field of building materials engineering" BPI/WTP/2021/1/00002, MATBUD'2023.

Conflicts of Interest: The authors declare no conflict of interest.

References

1. Shi, C.; Qu, B.; Provis, J.L. Recent progress in low-carbon binders. *Cem. Concr. Res.* **2019**, *122*, 227–250. [CrossRef]
2. Sonat, C.; Lim, C.H.; Liska, M.; Unluer, C. Recycling and reuse of reactive MgO cements–A feasibility study. *Constr. Build. Mater.* **2017**, *157*, 172–181. [CrossRef]
3. Unluer, C.; Al-Tabbaa, A. Enhancing the carbonation of MgO cement porous blocks through improved curing conditions. *Cem. Concr. Res.* **2014**, *59*, 55–65. [CrossRef]
4. Dung, N.T.; Lesimple, A.; Hay, R.; Celik, K.; Unluer, C. Formation of carbonate phases and their effect on the performance of reactive MgO cement formulations. *Cem. Concr. Res.* **2019**, *125*, 105894. [CrossRef]
5. Liska, M.; Al-Tabbaa, A. Ultra-green construction: Reactive magnesia masonry products. *Proc. Inst. Civ. Eng. Waste Resour. Manag.* **2009**, *162*, 185–196. [CrossRef]
6. Grünhäuser Soares, E.; Castro-Gomes, J. Carbonation curing influencing factors of Carbonated Reactive Magnesia Cements (CRMC)–A review. *J. Clean. Prod.* **2021**, *305*, 17. [CrossRef]
7. Humbert, P.S.; Castro-Gomes, J.P.; Savastano, H. Clinker-free CO_2 cured steel slag based binder: Optimal conditions and potential applications. *Constr Build. Mater.* **2019**, *210*, 413–421. [CrossRef]
8. Grünhäuser Soares, E.; Castro-Gomes, J.; Sitarz, M.; Zdeb, T.; Hager, I. The Immobilisation of Heavy Metals from Sewage Sludge Ash in CO_2-Cured Mortars. *Sustainability* **2021**, *13*, 12893. [CrossRef]
9. Grünhäuser Soares, E.; Castro-Gomes, J.; Sitarz, M.; Zdeb, T.; Hager, I.; Hassan, K.; Al-Kuwari, M.S. Feasibility for co-utilisation of Carbonated Reactive Magnesia Cement (CRMC) and industrial wastes in circular economy and CO_2 mineralisation. *Constr. Build. Mater.* **2022**, *323*, 13. [CrossRef]
10. Grünhäuser Soares, E.; Castro-Gomes, J. The role of biomass bottom ash in Carbonated Reactive Magnesia Cement (CRMC) for CO_2 mineralisation. *J. Clean Prod.* **2022**, *380*, 135092. [CrossRef]
11. Shand, M.A. *The Chemistry and Technology of Magnesia*; John Wiley & Sons, Inc.: Hoboken, NJ, USA, 2006. [CrossRef]
12. Jin, F.; Al-Tabbaa, A. Characterisation of different commercial reactive magnesia. *Adv. Cem. Res.* **2014**, *26*, 101–113. [CrossRef]
13. Ma, H. Mercury intrusion porosimetry in concrete technology: Tips in measurement, pore structure parameter acquisition and application. *J. Porous Mater.* **2014**, *21*, 207–215. [CrossRef]

14. Everett, D.H. Manual of Symbols and Terminology for Physicochemical Quantities and Units, Appendix II: Definitions, Terminology and Symbols in Colloid and Surface Chemistry. *Pure Appl. Chem.* **1972**, *31*, 577–638. [CrossRef]
15. Dung, N.T.; Unluer, C. Carbonated MgO concrete with improved performance: The influence of temperature and hydration agent on hydration, carbonation and strength gain. *Cem. Concr. Compos.* **2017**, *82*, 152–164. [CrossRef]
16. Wu, H.; Zhang, D.; Ellis, B.R.; Li, V.C. Mechanical behavior of carbonated MgO-based Engineered Cementitious Composite (ECC) after high temperatures exposure. *Cem. Concr. Compos.* **2021**, *124*, 104255. [CrossRef]
17. Hay, R.; Otchere, C.; Kashwani, G.; Celik, K. Recycling carbonated reactive magnesium cement (RMC) as a building material. *J. Clean Prod.* **2021**, *320*, 128838. [CrossRef]
18. Dung, N.T.; Unluer, C. Improving the performance of reactive MgO cement-based concrete mixes. *Constr. Build. Mater.* **2016**, *126*, 747–758. [CrossRef]
19. Unluer, C.; Al-Tabbaa, A. The role of brucite, ground granulated blastfurnace slag, and magnesium silicates in the carbonation and performance of MgO cements. *Constr. Build. Mater.* **2015**, *94*, 629–643. [CrossRef]
20. Bhattacharjya, D.; Selvamani, T.; Mukhopadhyay, I. Thermal decomposition of hydromagnesite. *J. Therm. Anal. Calorim.* **2012**, *107*, 439–445. [CrossRef]
21. Jauffret, G.; Morrison, J.; Glasser, F.P. On the thermal decomposition of nesquehonite. *J. Therm. Anal. Calorim.* **2015**, *122*, 601–609. [CrossRef]
22. Tian, L.; Tahmasebi, A.; Yu, J. An experimental study on thermal decomposition behavior of magnesite. *J. Therm. Anal. Calorim.* **2014**, *118*, 1577–1584. [CrossRef]
23. Thiery, M.; Villain, G.; Dangla, P.; Platret, G. Investigation of the carbonation front shape on cementitious materials: Effects of the chemical kinetics. *Cem. Concr. Res.* **2007**, *37*, 1047–1058. [CrossRef]
24. Tu, Z.; Guo, M.Z.; Poon, C.S.; Shi, C. Effects of limestone powder on $CaCO_3$ precipitation in CO_2 cured cement pastes. *Cem. Concr. Compos.* **2016**, *72*, 9–16. [CrossRef]
25. Qin, L.; Gao, X. Properties of coal gangue-Portland cement mixture with carbonation. *Fuel* **2019**, *245*, 1–12. [CrossRef]
26. Bhagath Singh, G.V.P.; Sonat, C.; Yang, E.H.; Unluer, C. Performance of MgO and MgO–SiO_2 systems containing seeds under different curing conditions. *Cem. Concr. Compos.* **2020**, *108*, 103543. [CrossRef]
27. Khalil, A.; Sohn, S.; Celik, K. Thermal properties and stability of reactive magnesia cement. *Constr. Build. Mater.* **2021**, *308*, 125102. [CrossRef]
28. Coleyshaw, E.E.; Crump, G.; Griffith, W. Vibrational spectra of the hydrated carbonate minerals ikaite, monohydrocalcite, lansfordite and nesquehonite. *Spectrochim. Acta Part A* **2003**, *59*, 2231–2239. [CrossRef]
29. Kloprogge, J.T.; Martens, W.N.; Nothdurft, L.; Duong, L.V.; Webb, G.E. Low temperature synthesis and characterization of nesquehonite. *J. Mater. Sci. Lett.* **2003**, *22*, 825–829. [CrossRef]
30. Nied, D.; Enemark-Rasmussen, K.; L'Hopital, E.; Skibsted, J.; Lothenbach, B. Properties of magnesium silicate hydrates (M-S-H). *Cem. Concr. Res.* **2016**, *79*, 323–332. [CrossRef]